Vitreous Fibrillar Structure and Interfibrillar Composition in Adult Mice

Patricia Jaramillo-Garcés,[1–3] Judit Pampalona,[4] Ana Carretero,[1–3] Eduard José Cunilleras,[5] David Ramos,[1,4] and Jesús Ruberte[1–3]

[1]Centre for Animal Biotechnology and Gene Therapy (CBATEG), Universitat Autònoma de Barcelona, Bellaterra, Spain
[2]CIBER for Diabetes and Associated Metabolic Diseases (CIBERDEM), Madrid, Spain
[3]Department of Animal Health and Anatomy, Faculty of Veterinary Medicine, Universitat Autònoma de Barcelona, Bellaterra, Spain
[4]Department of Morphological Sciences, Faculty of Medicine, Universitat Autònoma de Barcelona, Bellaterra, Spain
[5]Department of Animal Medicine and Surgery, Faculty of Veterinary Medicine, Universitat Autònoma de Barcelona, Bellaterra, Spain

Correspondence: Jesús Ruberte, CBATEG – Center for Animal, Biotechnology and Gene Therapy, Autonomous University of Barcelona, C/de la Vall Morona, Bellaterra (Cerdanyola del Vallès) 08193, Spain; jesus.ruberte@uab.cat.

Received: December 3, 2024
Accepted: February 26, 2025
Published: March 31, 2025

Citation: Jaramillo-Garcés P, Pampalona J, Carretero A, Cunilleras EJ, Ramos D, Ruberte J. Vitreous fibrillar structure and interfibrillar composition in adult mice. *Invest Ophthalmol Vis Sci.* 2025;66(3):60. https://doi.org/10.1167/iovs.66.3.60

Purpose. Although mice are widely used models for human eye diseases, knowledge of their vitreous is scarce and fragmentary. This study characterizes the structure and composition of vitreous fibrils and their interfibrillar space. Given the role of this fibrillar network in maintaining the vitreous' biomechanical properties, the impact of intravitreal injections on vitreous architecture was also explored.

Methods. Healthy adult C57/BL6J mice were studied. Classical histological techniques, picrosirius red-polarization, immunofluorescence, lectin histochemistry, and hyaluronic acid binding protein assays were used to examine vitreous fibrils and interfibrillar space. For the analysis of distribution of components along the fibrils, the Airyscan microscopy was used to achieve higher resolution.

Results. Vitreous fibrils consist of fibrillar collagen, glycoproteins (fibrillin 1, fibronectin, laminin, and collagen IV), N-acetyl galactosamine, and hyaluronan, all absent in the interfibrillar space. A single sterile intravitreal saline injection induced an inflammatory insult, characterized by increased fibril density and macrophage/hyalocyte invasion. Lysosome-associated membrane protein 1 (Lamp1) immunohistochemistry suggests these cells may remove fibrils via phagocytosis and activate a remodeling process in the vitreous.

Conclusions. This study enhances understanding of the mouse vitreous structure, suggesting fibrils are composed of glycoprotein-wrapped collagen cores. Furthermore, the absence of hyaluronan and glycoproteins between fibrils may explain lower viscosity in mice compared with humans. Intravitreal injections as an inflammatory insult disrupt fibril networks and activate macrophages/hyalocytes.

Keywords: vitreous fibrils, hyalocyte, macrophage, intravitreal injection, sterile inflammation

The vitreous is classically described as a gel-like extracellular matrix inside the eye.[1–3] This gel fills the cavity behind the lens and is adhered to the retina.[4,5] The vitreous maintains the shape of the eyeball[2,4,6] and provides the metabolic requirements of the lens. It serves as a barrier for the diffusion of large macromolecules[7,8] and plays a key role in coordinating eye growth.[9–11]

It has previously been established that in mammals a network of fibrils endows the vitreous with shape, strength, flexibility, and resistance to tractional forces.[12,13] These fibrils are heterotypic, consisting of a mixed composition containing collagen II, IX, and V/XI.[14] They are heterogeneously distributed across different regions of the vitreous, and present several configurations based on their aggregation relationships with other macromolecules present in the vitreous.[3,15–18] Additionally, charged carbohydrates, particularly glycosaminoglycans (GAGs) are found between fibrils. These GAGs attract water, generating a swelling pressure that separates collagen fibrils, inflates the vitreous, and withstands compressive forces.[4,17] The primary GAG between fibrils is hyaluronan (HA),[19,20] which entangles with vitreous collagen and with hyaluronan-binding macromolecules, including versican, aggrecan, and others,[21,22] to form the vitreous gel.[17] In addition, low-molecular-weight molecules, such as lipids, salts, sugars, and lactate, and, so far, more than 600 unique proteins have been also described in the vitreous.[23–25]

Despite being one of the most used eye disease models, the structure and composition of the adult mouse vitreous is still poorly understood. In comparison with humans, the mouse eye has a relatively large lens and a smaller vitreous, being its volume only 4.4 µL in C57BL/6 mice.[26] Further-

more, human vitreous exhibits a hydrogel-like consistency, whereas the mouse vitreous is comparatively less dense. Several studies about the developing vitreous,[4,9,27,28] as well as studies on its proteomic composition[29,30] have been published. However, only a few studies deal with the structure of the vitreous fibrils and the composition of the interfibrillar space,[27,31–34] which both determine the physical properties of the vitreous.

Intravitreal injections have become a prevalent intraocular therapeutic procedure globally, marking a significant advancement in the treatment of various conditions like age-related macular degeneration, diabetic macular edema, proliferative diabetic retinopathy, retinal vein occlusion, pathological myopia, and uveitis, among others.[35,36] However, due to the relatively short half-life of drugs injected into the vitreous, patients typically undergo a series of repeated injections,[35,37] which carry potential risks, producing mechanical injury that triggers intraocular inflammation.[37–39] Thus, a better understanding of the vitreous structure and composition, as well as the impact of the inflammatory insult caused by the intravitreal injections on this ocular structure, could help overcome pharmacological limitations related to drug interactions with vitreous components, ultimately improving therapeutic concentration and diffusion.

The primary objective of this study was to characterize the structure and composition of the adult mouse vitreous and analyze the impact of a mechanical injury provoked by an intravitreal injection on its integrity.

Materials and Methods

Mice

C57BL/6J male and female mice aged 20 weeks were used in this study. Twenty different eyes were used for the histological findings presented in the figures. The mice were maintained in the animal facility under controlled environmental conditions (20°C temperature, 60% humidity, and 12 hours of light/dark cycles) and provided with water and a standard diet ad libitum (2018S TEKLAD Global, Harlan Teklad, Madison, WI, USA). All mice were euthanized with an inhaled overdose of isoflurane or anesthetized with an intraperitoneal injection of ketamine (100 mg/kg) and xylazine (12 mg/kg) followed by cervical dislocation.

Experimental procedures were performed in accordance with the ARVO Statement for the Use of Animals in Ophthalmic and Vision Research and the ARRIVE (Animal Research: Reporting In Vivo Experiments) guidelines 2.0 and were approved by the Ethics Committee for Animal and Human Experimentation of the Universitat Autònoma de Barcelona (UAB; FUE-2018-00717286).

Hematoxylin-Eosin Staining in Paraffin Sections

The eyes were enucleated and fixed with a 10% neutral buffer formalin solution. Additionally, samples were dehydrated and cleared with ethanol and xylol series (Panreac) and embedded in paraffin. Sections of 5 µm thick were obtained with a Leica RM2125RT microtome passing through the optic axis of the eyeball. Then, deparaffinized and rehydrated eye sections were stained for 5 minutes with Harris Hematoxylin (Sigma-Aldrich) followed by a quick dip in 0.25% hydrochloric acid. Furthermore, the slices were washed with distilled water and incubated in Eosin for 1 minute. Sections were dehydrated and cleared with xylol before been mounted with DPX (Sigma Aldrich).

Table 1. Lectins Used and Their Major Carbohydrate Specificities

Lectin	Plant Source	Sugar Binding Specificity
RCA-I	*Ricinus communis*	β-GalNAc/β-Gal
SBA	*Glycine max*	α-GalNAc/Gal
WFA	*Wisteria floribunda*	β-GalNAc
UEA-I	*Ulex europeus*	Fuc
WGA	*Triticum vulgare*	β-GlcNAc; NeuAcNAc

Fuc, fucose; Gal, galactosamine; Glc, glucosamine; NAc, N-acetyl; NeuAC, neuroaminic acid.

Picrosirius Red Stain-Polarization Method

After deparaffinization and rehydration, eye sections were stained with Weigert's hematoxylin (Sigma Aldrich) for 10 minutes, followed by rinsing with tap water for 10 minutes. The sections were then exposed to a Picrosirius red solution (Sigma Aldrich) for 1 hour and 15 minutes, followed by 2 immersions in acidified water. Although Picrosirius red stain alone does not selectively bind collagen, polarized light was used to enhance the visualization of the collagen network.[40] Picrosirius red is an elongated birefringent molecule that binds to a variety of molecules in tissue sections, not just collagen. However, when bound to collagen, it aligns parallel to the collagen fibrils, greatly enhancing their natural birefringence. Therefore, complexes of fibrous collagen bound Picrosirius Red exhibits much higher birefringence than complexes formed with other proteins. Picrosirius Red-bound fibrous collagen can then be detected under polarized light.

Periodic Acid Schiff

To detect mucopolysaccharides after deparaffinization and rehydration, sections were treated with 5% Periodic acid (Panreac) for 10 seconds, followed by incubation with Schiff's Reagent (Sigma Aldrich) for 30 minutes at 4°C. Afterward, the sections were counterstained with Harris Hematoxylin for 10 minutes before dehydration and mounting with DPX.

Lectins Histochemistry

The lectins used in this study and their specific binding sites are listed in Table 1. RCA-I (B1085), SBA (B1015), and WFA (B1355) were purchased from Vector Laboratories. WGA (L5142) and UEA-I (L8262) were obtained from Sigma Aldrich. Deparaffinized eye sections were rinsed in wash buffer and incubated with biotinylated lectins diluted in PBS + 0.1% Triton X-100 + 0.1 mM CaCl2, MgCl2, and MnCl2 overnight at 4°C. The lectin concentration used in all cases was 20 to 25 µg/mL to achieve maximum staining with minimal background. After several rinses, the sections were incubated with streptavidin Alexa Fluor 488 conjugate. Nuclei were counterstained with Hoechst (Sigma Aldrich) for 5 minutes at room temperature, rinsed, and mounted with Fluoromount. Negative controls were performed on sequential tissue sections by omitting the corresponding lectin.

Investigative Ophthalmology & Visual Science

Hyaluronan Detection by Biotinylated Hyaluronic Acid Binding Protein

Eye sections were subjected to deparaffinization and rehydration, followed by three successive washes with PBS. Samples were then blocked with a solution of PBS, 0.05% Igepal, and 10% goat serum for 45 minutes. Biotinylated hyaluronic acid binding protein (b-HABP, 385911; Sigma Aldrich) was applied overnight at 4°C, at a dilution of 1:100. Two types of controls were implemented: one involved replicating the procedure while excluding the application of b-HABP, and the other involved pretreating the samples with Hyaluronidase (H3884; Sigma Aldrich) at 37°C for 30 minutes before incubation with b-HABP. The following day, the samples were rinsed and incubated with Streptavidin Alexa Fluor 488 conjugate secondary antibody for 30 minutes. Nuclei were counterstained with Hoechst for 10 minutes before mounting with Fluoromount.

Immunofluorescence

Deparaffinized and rehydrated sections underwent antigen retrieval to expose epitopes. Sections were blocked with a solution of PBS, 0.05% Igepal, and 10% goat serum for 45 minutes. They were then incubated overnight at 4°C with primary antibodies, all diluted in the blocking solution. The primary antibodies used included rabbit anti-mouse Fibrillin1 (1:100; ab53676; Abcam), rabbit anti- mouse Fibronectin (1:100; Sigma/F3648), rabbit anti-mouse collagen IV (1:20; AB769; Merck Millipore), rabbit anti-mouse Laminin (1:200; Z0097; DAKO, Glostrup, Denmark), rat anti-MAC2 (1:50; Cedarlane CL8942AP), and rat anti-lysosome-associated membrane protein 1 (Lamp1; 1:50; Santa Cruz; SC18821). After several rinses in blocking solution, the sections were incubated with goat anti-rabbit Alexa 488 or 568 secondary antibody (1:100; A11008; Invitrogen) for 2 hours at room temperature. Sections were counterstained with Hoechst (Sigma Aldrich) for 10 minutes and mounted in Fluoromount. Negative controls were performed by omitting the primary antibody in sequential tissue sections.

Confocal Fluorescence Imaging Acquisition and Analysis

Image acquisition was carried out using a SP5 laser scanning confocal microscope (Leica Microsystems GmbH, Heidelberg, Germany). Subsequent image processing and analysis were conducted using ImageJ/Fiji.[41] To determine the location of the fluorescence signal and differentiate between the vitreous fibrils and their interfibrillar space, the correspondence between the fluorescence signal and the vitreous fibrils observed by bright-field microscopy was always established (Supplementary Fig. S1). For the analysis of glycoprotein distribution within the vitreous fibrils, Airyscan mode on a Zeiss Confocal 980 was used to achieve higher resolution. This enhanced resolution was also used to assess the colocalization of fibrillin 1 and Lamp1. To evaluate their degree of colocalization, 7 independent experiments using ImageJ (Fiji) and Zeiss Confocal 980 software were analyzed. Fluorescence patterns were analyzed using the Pearson correlation coefficient and Manders' overlap coefficient (M1) to quantify colocalization. Both global and region-specific (rectangular) analyses were performed, with weighted colocalization coefficients calculated for each channel.

Intravitreal Sterile Isotonic Saline Injection

Mice were injected subcutaneously with the analgesic Buprenex (10 µL/g, Indivor) and then anesthetized with an intraperitoneal injection of xylazine (12 mg/kg) and ketamine (100 mg/kg). To prevent corneal dryness, Viscofresh drops (Allergan) were applied, along with topical anti-inflammatory and antibiotic TobraDex (Alcon). For the intravitreal injection ($n = 6$) of 7 µL isotonic saline (Lactato-RingerVet), a Hamilton syringe was used (HA-80300 Teknokroma) with a capacity of 10 µL, and 0.47 mm needle diameter. The injection was administered through the posterior segment of the eye, with the needle inserted at a 45 degrees angle through the corneoscleral limbus. To minimize the risk of lens damage, a sterile eyelid speculum was used to ensure proper alignment and maintain a clear injection trajectory. Post-procedure imaging confirmed that the lens remained unharmed.

Twenty-four hours after injection, the mice were euthanized, their eyes were enucleated, fixed, and processed for paraffin embedding, following a previously described protocol.

Results

Topography and Distribution of Vitreous Fibrils

Vitreous fibrils were visible as a sparse thin network using conventional hematoxylin and eosin (H&E) staining on paraffin sections (Fig. 1) in the retrolental, vitreoretinal, and zonular areas, corresponding to the central, basal, and vitreous cortex described by Boos et al. in humans.[42] The Picrosirius red stain combined with polarized light detection (PSR-POL), one of the best understood histochemical techniques to detect fibrous collagen,[40] revealed glittering lines in the vitreous fibrils, confirming the presence of fibrous collagen in their structure (see Fig. 1). This finding is consistent with previous study showing that collagen II, one of seven fibrillar collagens found in animals[43,44] is the primary fibrillar component of the mouse vitreous.[27,45] The thickness of vitreous fibrils observed by PSR-POL (0.06 ± 0.02 µm: $n = 15$) matched the known thickness of fibrous collagen.[46]

Based on the 2D images of vitreous fibril obtained from 5 µm thickness paraffin sections after PSR-POL, several observations on their geometric structure can be stated. First, the fibrils had a roughly constant diameter which was several orders of magnitude smaller than their length. Some fibrils extended beyond approximately −24 µm in length, which represents a lower bound on the actual maximum extension of these fibrils. This is because the measurements were made using 2D images which are projections of the 3D fibrils onto the image plane. Therefore, if a fibril is not exactly contained within a plane parallel to the image (which is an extremely unlikely situation), the observed length was shorter than the actual length (Fig. 2). Additionally, it is possible that a given vitreous fibril was not fully captured within a 2D image. If the fibril enters and/or exits the paraffin section at different points, this will not be apparent from the micrographs (see Fig. 2), again, leading to an underestimation of the fibril's length. For instance, a fibril crossing the paraffin section orthogonally would appear as a point in the 2D images (see Fig. 2). Furthermore, the 2D projection of the fibril may have additional effects. It is plausible that certain fibrils bend or branch in intricate ways (see Fig. 2), which may result in the appearance of blurred fibrils in the micrographs.

Investigative Ophthalmology & Visual Science

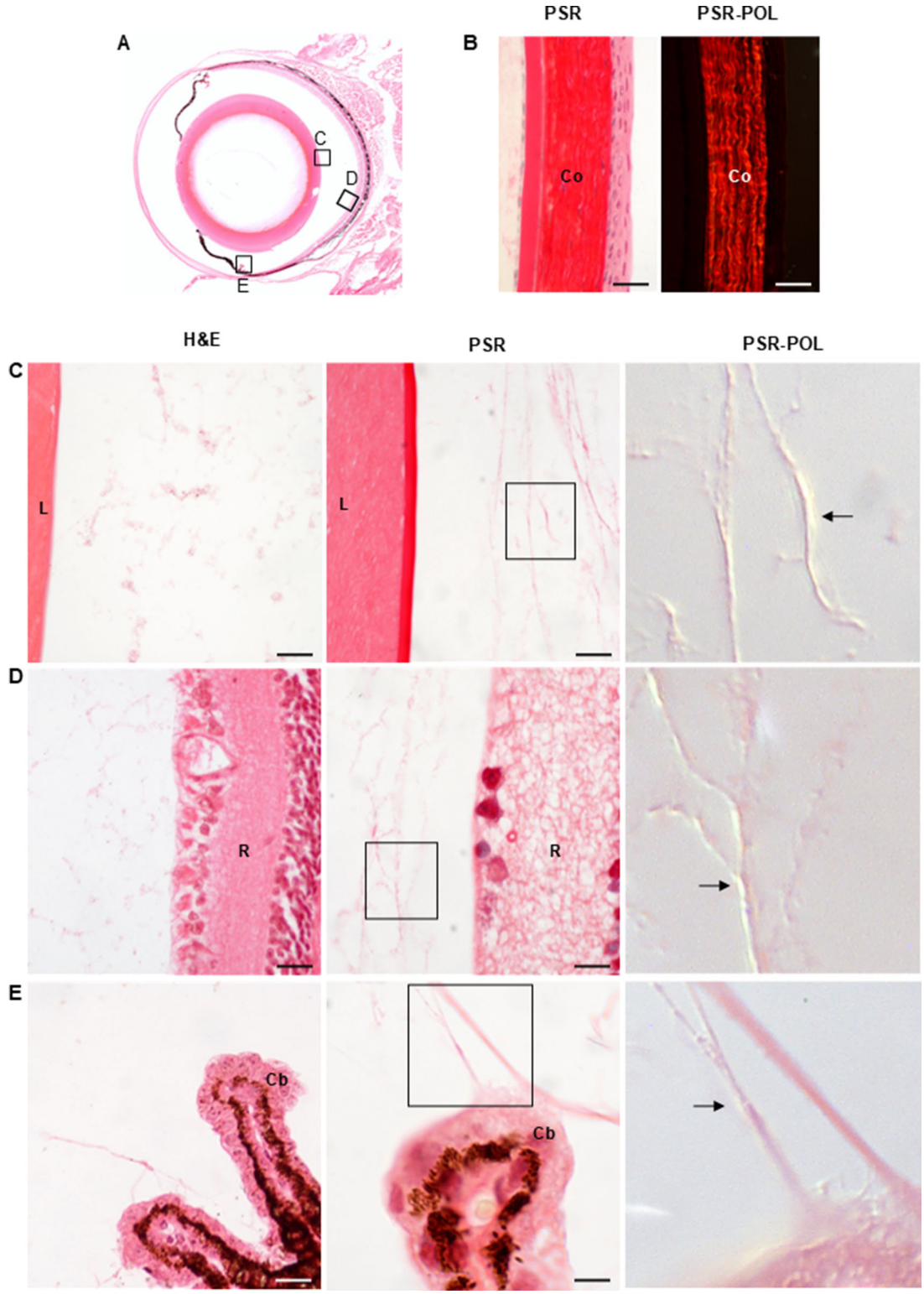

Figure 1. Topography and distribution of vitreous fibrils. (**A**) Section through the optic axis of a mouse eye stained with H&E showing the areas magnified below. (**B**) The polarized light clearly identified the glittering collagen fibers stained with picrosirius red in the cornea. Fibrillar collagen was evident in the vitreous fibrils at the retrolental (**C**), vitreoretinal (**D**), and zonular (**E**) areas. Picrosirius red staining evidenced more clearly the vitreous fibrils that the H&E staining (compare *left and central panels*). Zonular fibrils appeared less glittery than retrolental and vitreoretinal fibrils suggesting less fibrillar collagen present in its composition. PSR, Picrosirius red; PSR-POL, Picrosirius red-polarized light; L, lens; R, retina; Cb, ciliary body; Co, cornea. Scale bars = 26.61 µm (**B**); 23.30 µm (**C** *left panel*); 13.61 µm (**C** *central panel*); 24.09 µm (**D** *left panel*); 9.42 µm (**D** *central panel*); 29.36 µm (**E** *left panel*); 15.76 µm (**E** *central panel*).

Investigative Ophthalmology & Visual Science

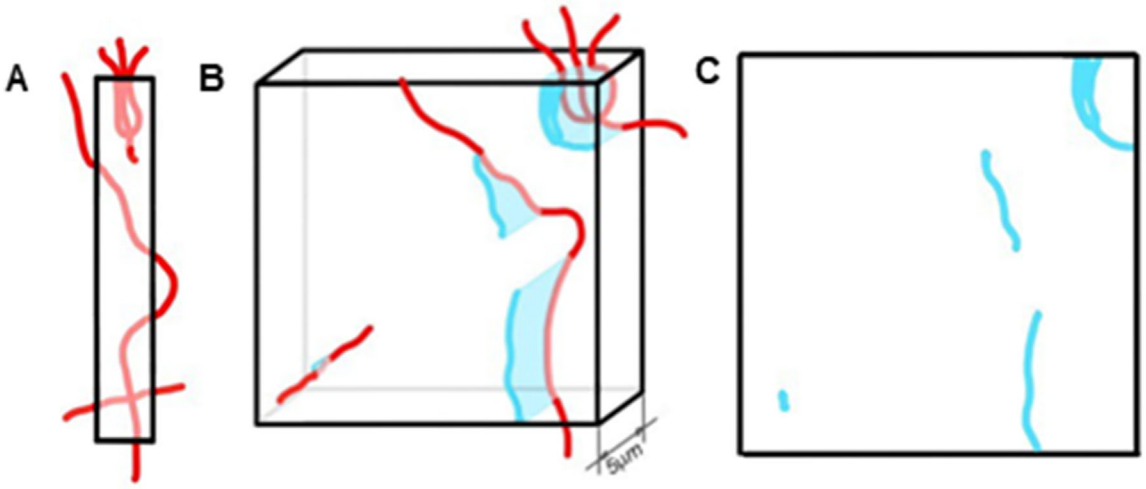

Figure 2. Schematic representation of a paraffin section of the vitreous containing fibrils (*red*). (**A**) Side view of the section. (**B**) Three-dimensional view of the section including the projections of the fibrils (*light blue*). (**C**) Actual image observed through the microscope.

Vitreous Fibrils and Interfibrillar Space Protein Composition

In addition to the fibrous collagen detected by PSR-POL, immunofluorescence revealed other non-fibrous proteins in the mouse vitreous fibrils: fibrillin 1, fibronectin, laminin, and collagen IV (Fig. 3, Supplementary Figs. S2, S3). Fibrillin 1, a large cysteine-rich glycoprotein, was found in the retrolental, vitreoretinal, and zonular areas. Previously, fibrillin 1 had been only reported as a component of the zonular fibers.[32] Fibronectin, a glycoprotein that interacts with cell surface receptors such as integrins and syndecans,[47–49] was also present in the retrolental, vitreoretinal, and zonular fibrils. Furthermore, the cell adhesion protein laminin, a heterotrimeric glycoprotein composed of α, β, and γ chains,[17,47] was associated with the retrolental, vitreoretinal, and zonular fibrils. Laminin is a well-known component of the retinal inner limiting membrane, which forms the boundary between the retina and the vitreous.[50,51] Finally, collagen IV, the primary non-fibrillar component of the basement membranes, typically associated to fibronectin and laminin,[52] was also present in the retrolental, vitreoretinal, and zonular fibrils. Laminin and collagen IV have previously been described as components of the intravitreal membrane, a membranous structure that separates the primary and secondary vitreous at postnatal day 4 in the mouse.[9]

The thickness of vitreous fibrils measured on immunofluorescent images was consistently greater than the thickness of fibrils measured using PSR-POL (Fig. 4), suggesting that fibrillin 1, fibronectin, laminin, and collagen IV are wrapping a core of fibrillar collagen within the vitreous fibrils. The shape and morphology of vitreous fibrils appeared similar but not identical when the images of fibrillin 1, fibronectin, laminin, and collagen IV were compared (see Fig. 3, Supplementary Figs. S2, S3). This could indicate that the protein arrangement along the fibrils is not homogenous. To test this hypothesis, the Airyscan detector, which offers enhanced resolution for visualizing proteins on immunofluorescent slides, was used. Analysis of the fibrillin 1 arrangement along vitreous fibrils confirmed that fibrillin 1 was circumscribed to specific locations along vitreous fibrils (Fig. 5).

Under our experimental conditions, vitreous proteins were found exclusively associated with vitreous fibrils. No specific signal for these proteins was detected in the interfibrillar space (see Fig. 3, Supplementary Figs. S2, S3).

Vitreous Fibrils and Interfibrillar Space Carbohydrate Composition

Periodic Acid Schiff (PAS) staining is a widely used method to detect carbohydrates.[53] Our results showed the classical red PAS-positive reaction in the retrolental, vitreoretinal, and zonular areas (Fig. 6A). This is consistent with the fact that fibrillin 1, fibronectin, and laminin, which are detected in vitreous fibrils, are glycoproteins. To specifically identify these carbohydrates in the vitreous fibrils and in the interfibrillar space, lectin histochemistry was performed. GalNAc, an O-linked sugar to serine and threonine residues, was detected in the retrolental, vitreoretinal, and zonular fibrils using RCA-I, SBA, and WFA lectins (Fig. 6B, Supplementary Figs. S4, S5). Although RCA-I, SBA, and WFA lectins recognized the GalNAc monosaccharide, they displayed subtle differences in their signal intensities on mouse vitreous fibrils, likely due to their different binding specificities for α and β recognition domains (see Table 1).[54] A previous study showed that RCA-I and SBA bound to the hyaloid vessels and the primary vitreous fibrils at postnatal day 0 in the mouse.[9] Consistent with our findings, this study also observed differences in the signal intensities of RCA-I and SBA.

Fucose is unique in having an L-configuration, whereas all other naturally occurring monosaccharides in mammals exist in the D-conformation.[55] Fucosyl residues, specifically detected by UEA-I lectin, have been previously described binding to zonular fibrils of mice, rabbits, and humans.[56] Our results using UEA-I lectin confirmed this finding in mouse (see Supplementary Fig. S5). However, in contrast to findings in rabbits and humans, no fucose residues were associated with retrolental vitreous fibrils in mice (see Fig. 6B).

WGA lectins recognize the monosaccharide GlcNAc.[57,58] The vitreous fibrils in the retrolental and vitreoretinal areas, as well as the zonular fibrils, were positive for WGA, suggesting that HA, which contains GlcNAc in its composition,[59–61]

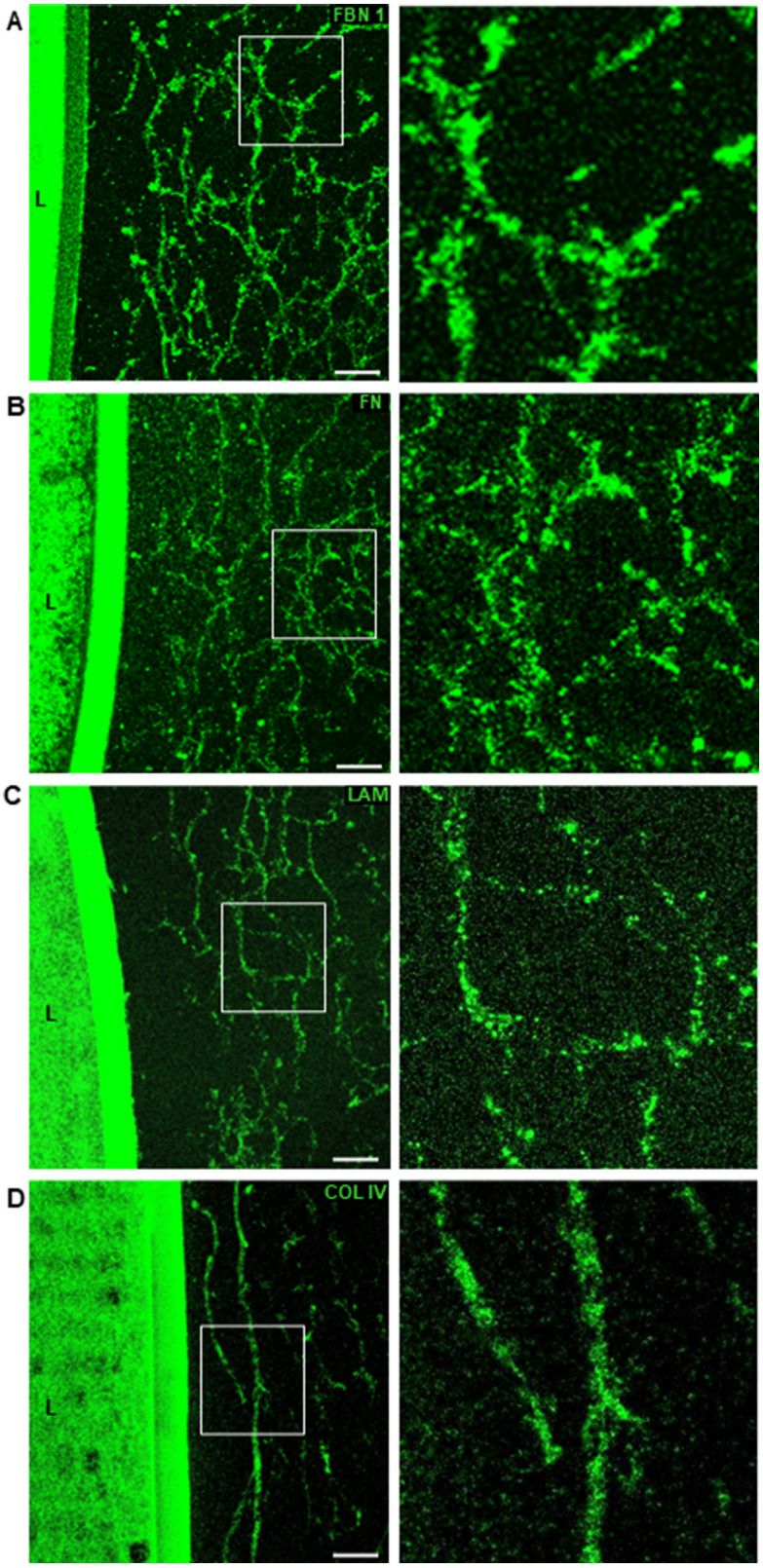

Figure 3. Vitreous fibrils and interfibrillar space protein composition. FBN 1 (**A**), FN (**B**), LAM (**C**), and COL IV (**D**) were found in the vitreous and zonula fibrils. Note that the shape and thickness of the fibrils are similar but not identical depending on the protein analyzed. None of the proteins analyzed were found between fibrils. FBN 1, fibrillin 1; FN, fibronectin; LAM, laminin; COL IV, Collagen IV; L, Lens. Scale bars = 18.70 µm (**A**); 17.5 µm (**B**); 15.10 µm (**C**); 12.92 µm (**D**).

Investigative Ophthalmology & Visual Science

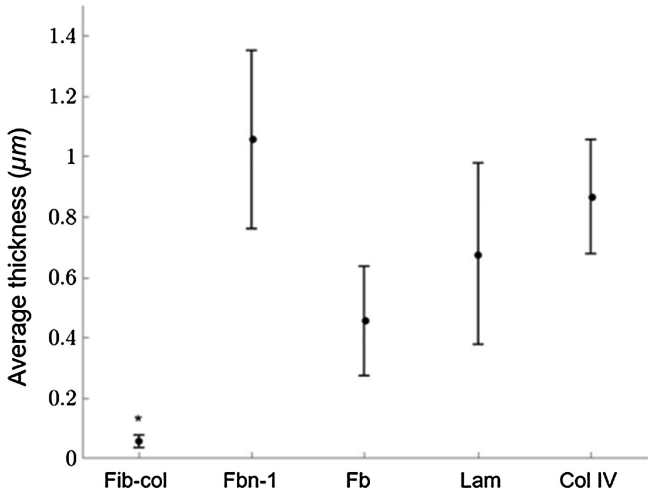

Figure 4. Average fibril thickness from protein visualization images. Vitreous fibrils visualized by Picrosirius red-polarized light were significantly smaller than when other proteins were used (0.06 ± 0.02 µm in PRS-POL) versus (1.06 ± 0.29 µm in Fbn1; $P = 0.0025$; $n = 24$); (0.46 ± 0.18 µm in Fn; $P = 0.039$; $n = 19$); (0.68 ± 0.30 µm in Lam; $P = 0.052$; $n = 21$); (0.87 ± 0.18 µm in Col IV; $P = 0.01$; $n = 25$).

is a component of these fibrils (Fig. 6C). In contrast, no WGA staining was observed in the interfibrillar space (see Fig. 6C). Supporting the hypothesis of HA being present in vitreous fibrils, previous studies have shown that WGA can also bind NeuNAc, another component of HA.[61,62] In our study, the lens capsule, retinal inner limiting membrane, and ciliary epithelium were also positive for WGA (see Fig. 6C).

To further assess whether vitreous fibrils are unequivocally composed of HA, because GlcNAc is not exclusive to HA and is also found in other carbohydrates,[63] we tested a b-HABP, which specifically binds HA.[64] Because previous studies have shown that HA is removed from the samples during formalin fixation, and that the acid-formalin/ethanol (Fekete's) fixative preserves HA better, we compared the HA signal in samples fixed with either NBF or Fekete's solution. No significant differences in HA fluorescent signals were observed between the two fixation methods (Supplementary Fig. S6). The results obtained using bHABP unequivocally showed that HA is a component of the vitreous and zonular fibrils in mice, but it was absent from the interfibrillar space (Fig. 7). Moreover, the HA signal faded from the vitreous chamber following treatment with hyaluronidase, further confirming the presence of HA in the vitreous fibrils. This finding in the mouse contradicts the general assumption that vitreous fibrils are surrounded by a network of HA, as observed, for example, in humans.[4,45]

Fibril Alteration After Intravitreal Injection

Intravitreal injections are one of the most common intraocular treatments worldwide due to their effectiveness in treating various retinal diseases, and had demonstrated been a secure clinical procedure.[35,37,65] Nevertheless, any intravitreal injection represents a mechanical injury that can trigger an inflammatory response in the surrounding tissue. To evaluate the injury effect of intravitreal injections in the fibrillar composition of mouse vitreous, a sterile injection of isotonic saline was administered through the sclera, targeting the posterior region of the lens. This procedure was not intended to replicate therapeutic intravitreal injections performed in humans but rather assess the vitreous reaction to an inflammatory insult (Fig. 8A).

Twenty-four hours post-injection, an increased density of fibrils was observed in the vitreous chamber (Fig. 8B). Simultaneously, a high number of single cells were found between the vitreous fibrils (see Fig. 8B). Further analysis using anti-Mac2 (CD11b) antibody, a specific marker of macrophages,[66] confirmed the macrophage-like nature of these cells (Fig. 8C). Given that hyalocytes also express this marker,[67] we suggest that the cells that increased in number within the vitreous after injection could be hyalocytes. The number of hyalocytes/macrophages was quantified in five of the non-injected eyes used as controls and in four of the injected ones. Cells were counted in the three specifics areas where the vitreous fibrils were previously analyzed (retrolental, vitreoretinal, and zonular). The injected group showed more variability in the number of found hyalocyte/macrophages (Table 2), suggesting that eyes responded differently to the injection, possibly due to variations on the inflammatory response.

Interestingly, in the injected eyes, always the number of hyalocyte/macrophages was higher in the vitreoretinal area, suggesting that vitreous macrophages could migrate from the retina. Despite this variability, the *t*-test revealed a statis-

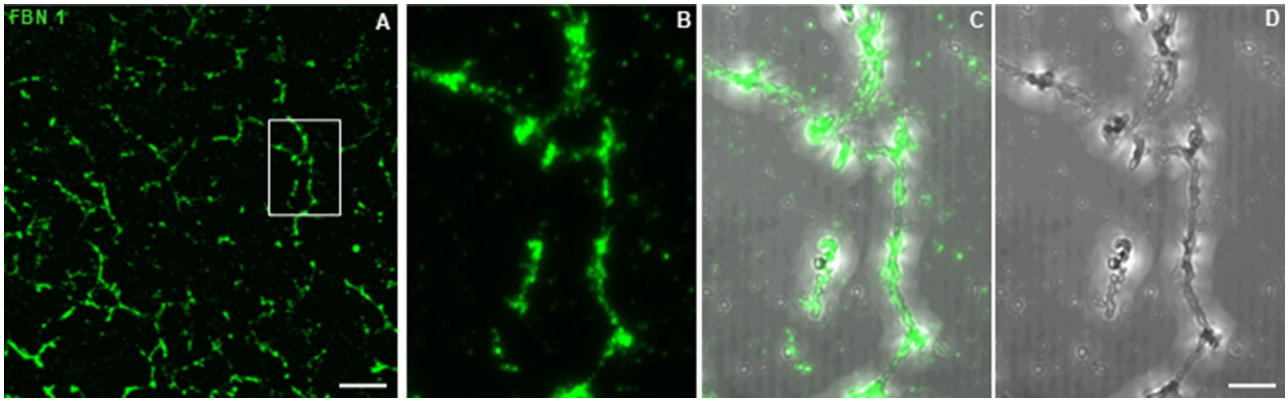

Figure 5. Fibrillin1 deposition on the vitreous fibrils observed by Airyscan microscopy. (**A**) Vitreous fibrils marked with anti-Fibrillin 1 in the retrolental area. (**B**) Enlargement showing the discontinuous appearance of Fibrillin 1 on the fibril. (**C**) Merged Fibrillin 1 signal and brightfield. (**D**) Brightfield showing the shadow of the complete fibril. FBN 1, fibrillin 1. Scale bars = 16.84 µm (**A**); 3.72 µm (**D**).

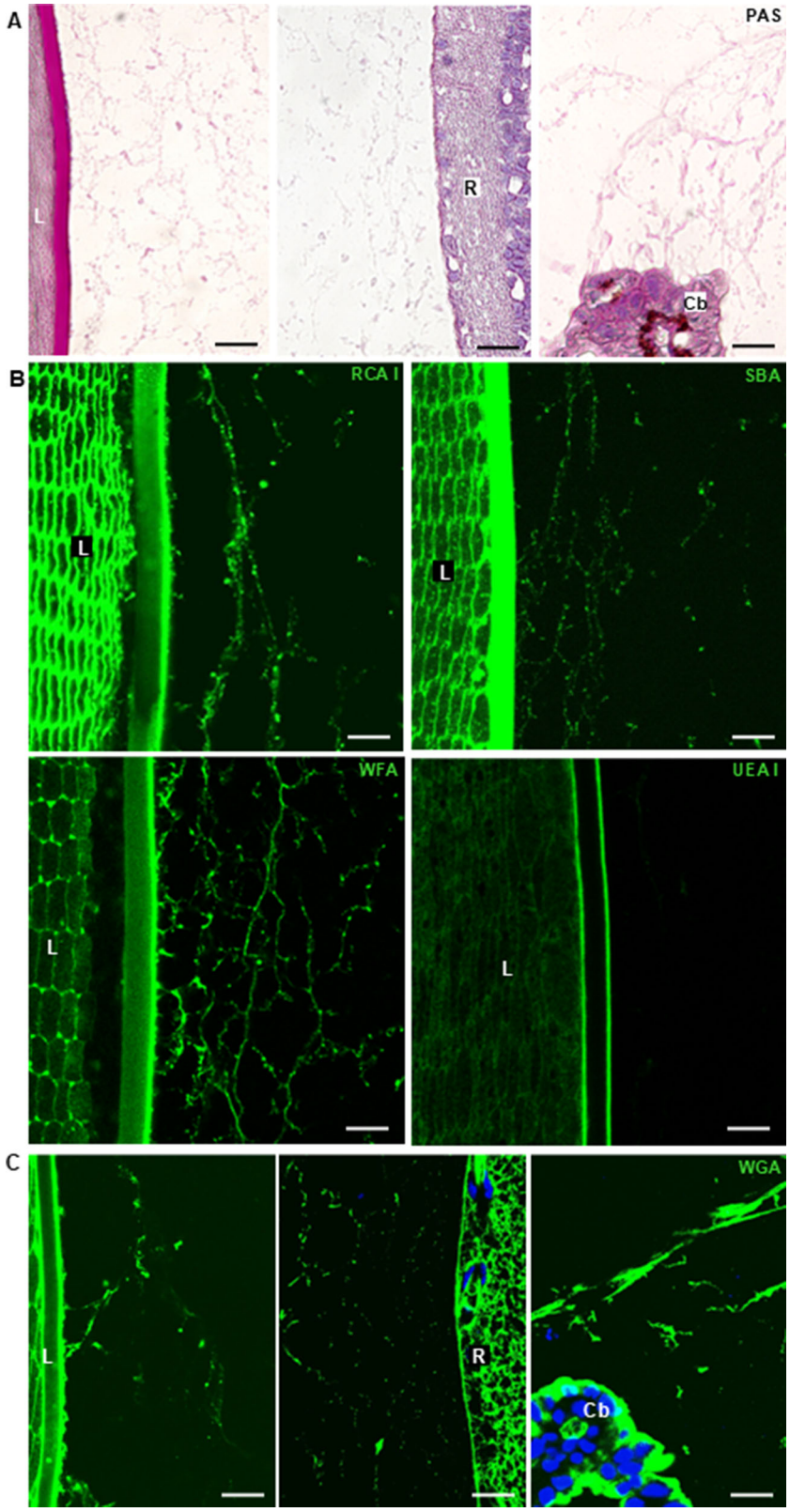

Figure 6. Vitreous fibrils and interfibrillar space carbohydrate composition. (**A**) Retrolental (*left*), vitreoretinal (*central*), and zonular fibrils (*right*) stained with PAS confirmed the presence of carbohydrate residues in the vitreous and zonular fibrils. (**B**) Positive RCA I, SBA, WFA, and UEA I staining on fibrils of the retrolental area. UEA I did not mark vitreous fibrils, indicating the absence of Fucose sugar. No carbohydrate signal was observed in the interfibrillar space. (**C**) WGA detecting GlcNAc/NeuNAc in retrolental, vitreoretinal, and zonular fibrils. This signal suggested the presence of hyaluronan in these fibrils. PAS, Periodic Acid-Schiff; RCA I, Ricinus communis; SBA, Soybean Glycine max; WFA, Wisteria floribunda; UEA I, Ulex europaeus; WGA, Wheat germ agglutinin; L, lens; R, retina; Cb, ciliary body. Scale bars = 27.30 µm (**A** *left panel*); 27.28 µm (**A** *central panel*); 26.42 µm (**A** *right panel*); 9.45 µm (**B** *top left panel*); 12.54 µm (**B** *top right panel*); 9.08 µm (**B** *bottom left panel*); 8.34 µm (**B** *bottom right panel*); 11.26 µm (**C** *left panel*); 15.05 µm (**C** *central panel*); 15.48 µm (**C** *right panel*).

Investigative Ophthalmology & Visual Science

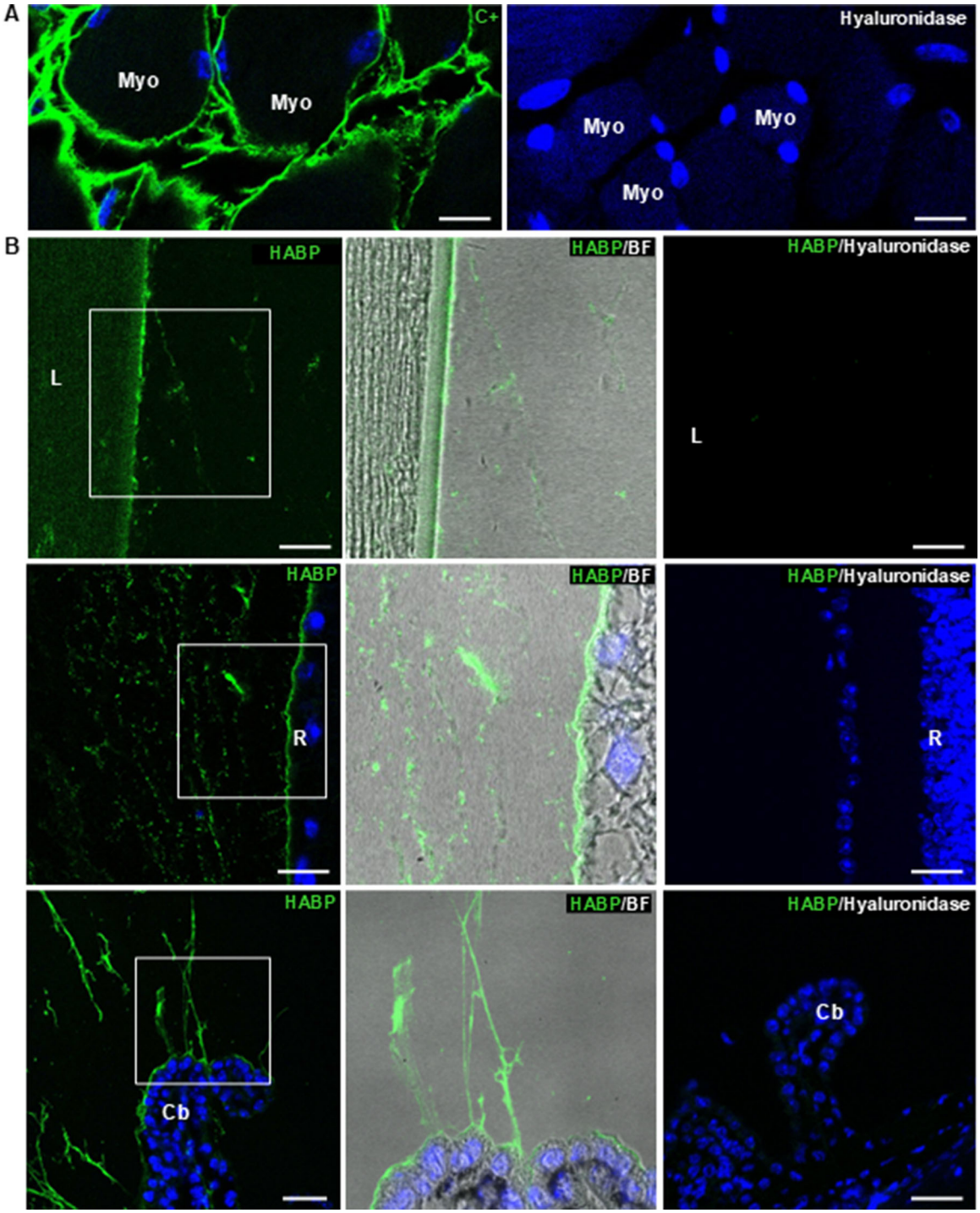

Figure 7. Detection of hyaluronan in the vitreous. (**A**) Positive control confirmed in extraocular muscles, where hyaluronan is a well-known component of the endomysium. The *right panel* shows the muscle pretreated with hyaluronidase, displaying no hyaluronan signal. (**B**) retrolental, (**C**) vitreoretinal, and (**D**) zonular areas were probed with HABP to demonstrate the localization of hyaluronan. The *left panels* show hyaluronan in a fibrillar arrangement. The *center panels* confirmed hyaluronan as part of the vitreous fibrils. The *right images* show the same eye areas pretreated with hyaluronidase. No hyaluronan was found in the interfibrillar space. HABP, hyaluronic acid binding protein; BF, bright field; L, lens; Myo, myocyte; R, retina; Cb, ciliary body. Scale bars = 12.79 µm (**A** *left panel*); 9.20 µm (**A** *right panel*); 16.45 µm (**B** *top left panel*); 16.5 µm (**B** *top right panel*); 15.21 µm (**B** *central left panel*); 27.55 µm (**B** *central right panel*); 39.04 µm (**B** *bottom left panel*); 31.48 µm (**B** *bottom right panel*).

tically significant difference ($P = 0.010$) between the injected and the control groups.

The cytoplasm of the hyalocytes found in the injected eyes contains fibrillin 1 (see Fig. 8B) and fibronectin (data not shown), suggesting that these cells were either phagocytosing the excess of vitreous fibrils produced after injection or, alternatively, were responsible for producing the vitreous fibrillar material. To elucidate between these two hypothe-

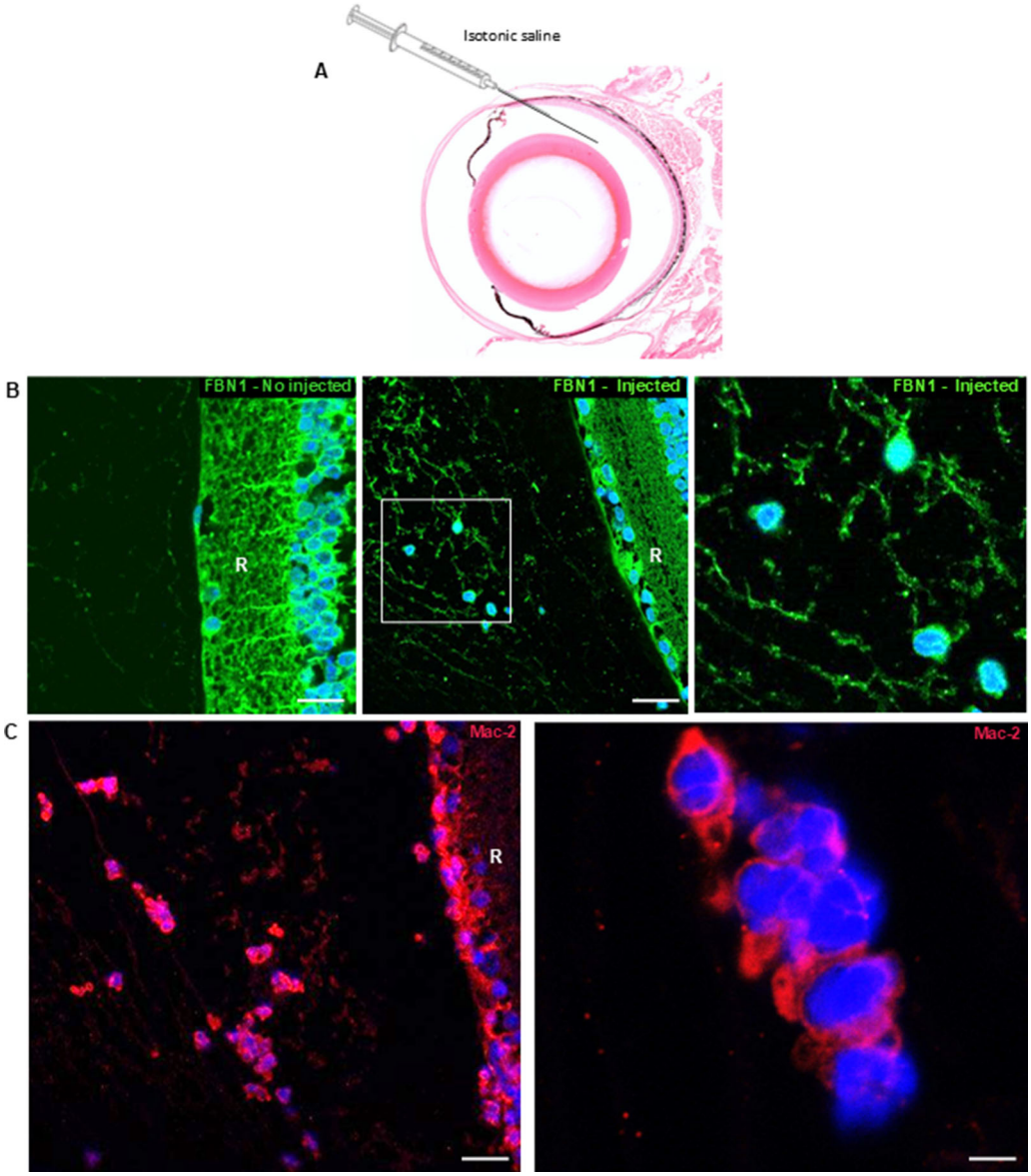

Figure 8. Increased higher fibril density and macrophages in vitreous injected with sterile isotonic saline. (**A**) Schematic figure showing the location of the sterile intravitreal injection. (**B**) The *left panel* shows the vitreoretinal area of a non-injected eye labeled with FBN 1. No cells are visible in the vitreous, and the fibril density is consistent with our previous results. The *center panel* shows the hyalocytes, appearing in the vitreous after injection. Additionally, fiber density seems higher compared with non-injected eyes. The *right panel* details the intravitreal cells and fibrils. Note that FBN 1 is present inside the cells. (**C**) The Mac-2 signal confirmed that intravitreal cells are macrophages. The *right panel* provides a detailed view of these macrophages. FBN 1, fibrillin 1; Mac-2, Galectin 3; R, retina. Scale bars = 18.34 µm (**B** *left panel*); 25.12 µm (**B** *central panel*); 19.34 µm (**C** *left panel*); 3.85 µm (**C** *right panel*).

Table 2. Number and Location of Hyalocytes/Macrophage Cells in the Vitreous

	No. of Hyalocytes/Macrophages				
Mouse Identification	**Retrolental**	**Vitreoretinal**	**Zonular**	**Total**	**Mean and SD**
1-C57BL/6J -Wt	2	1	3	6	7 ± 2.36
2-C57BL/6J -Wt	4	2	1	7	
3-C57BL/6J -Wt	3	1	4	8	
4-C57BL/6J -Wt	7	2	1	10	
5-C57BL/6J -Wt	2	2	4	8	
6-C57BL/6J -Wt	1	0	2	3	
7-C57BL/6J-Injected	10	26	12	48	46.25 ± 13.81
8-C57BL/6J-Injected	15	39	11	65	
9-C57BL/6J-Injected	12	17	9	38	
10-C57BL/6J-Injected	7	19	8	34	

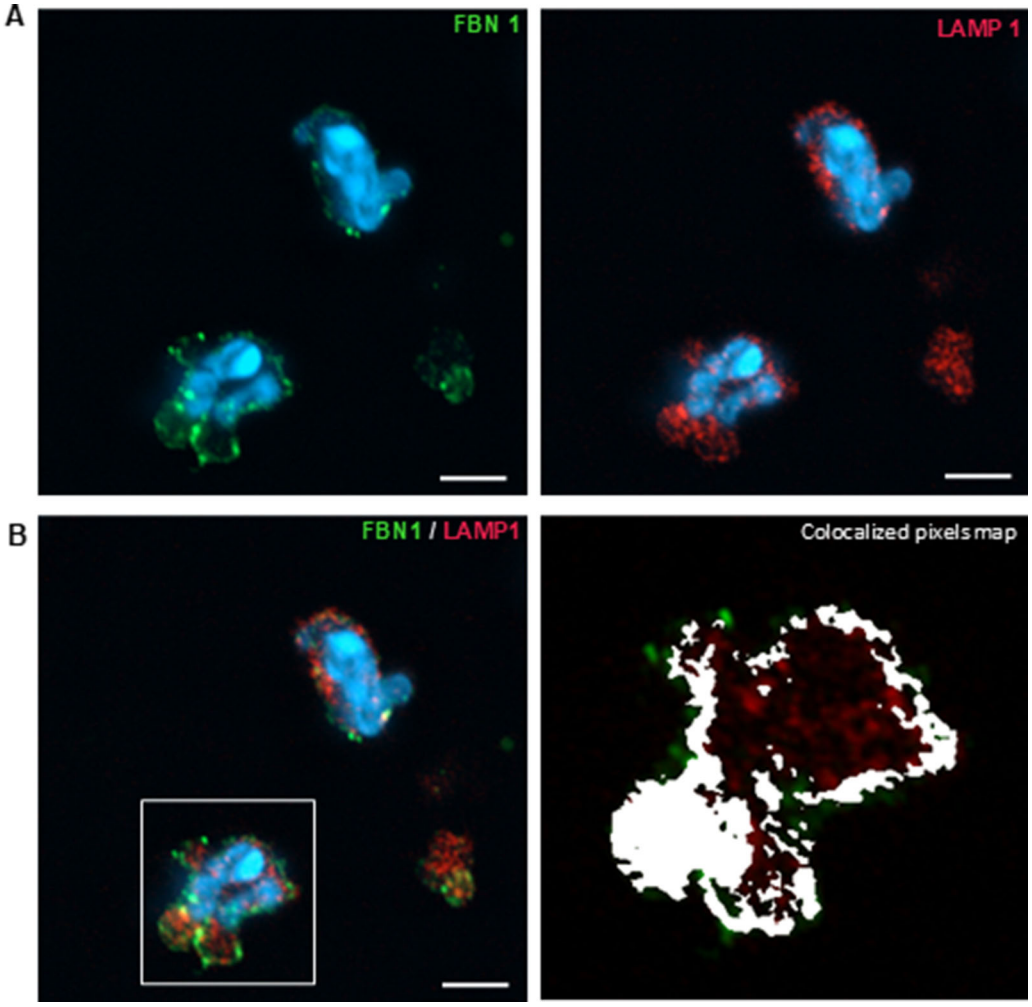

Figure 9. Colocalization of FBN 1 and Lamp1 in intravitreal macrophage cells. (**A**) Shows the two signals analyzed separately. (**B**) Shows the colocalization of both channels. On the *left*, is the complete merged image, displaying the overlap of both channels in certain areas of the cytoplasm. On the *right*, is the pixel colocalization map. FBN 1, fibrillin 1. Scale bars = 3.39 µm (**A** *left and right panels*, **B** *left panel*).

ses, we analyzed the hyalocytes found in the vitreous using Lamp1, one of the most abundant proteins in the lysosomal membrane[68] and involved in the degradation of extracellular material delivered to lysosomes via endocytosis.[69]

The colocalization analysis of fibrillin 1 and Lamp1 signals in the cytoplasm of hyalocytes revealed a high correlation between the two fluorophores. Pearson coefficients ranged from −0.00067 to 0.34572 (SD ± 0.1548), whereas Manders' coefficients varied from 0.42062 to 0.90400 (SD ± 0.0289). Additionally, pixel colocalization percentages spanned from 20.37% to 33.11%, indicating that fibrillin 1 was present inside the secondary lysosomes. These findings suggest a possible role for hyalocytes in phagocytosing the excess vitreous fibrils produced after intravitreal injections (see Fig. 9).

Discussion

Previous studies of the mouse vitreous have either focused on its development[4,9,70] or on proteomic analyses.[4,17,45] In this study, we have analyzed the structure and composition of the adult mouse vitreous using a variety of histological staining techniques and fluorescence confocal 2D microscopy.

The vitreous is considered as a part of the extracellular matrix, composed primarily of water (>90%) along with solid fibrillar components, such as collagen, proteoglycans and glycosaminoglycans.[4] Detailed studies on vitreous collagen have identified that the majority consists of thin, uniform fibrils composed of collagen types II, IX, and V/XII.[45,71,72] Other collagen variants, including types V and XI, although less abundant (10–25%), also contribute to the fibrils structure.[13,14] In our study, the use of Picrosirius red staining combined with polarized light detection confirmed the presence of fibrillar collagen in the vitreous fibrils across the retrolental, vitreoretinal, and zonular areas of the mouse eye. Additionally, immunofluorescence revealed the presence of fibrillin 1 (previously identified in the vitreous of humans, chickens, and cows),[4,73,74] as well as fibronectin,[47–49,75] laminin, and collagen IV as integral components of vitreous fibrils structure in mouse. Interestingly, the thickness of vitreous fibrils observed in our study suggests that fibrillin 1, fibronectin, laminin, and collagen IV might be surrounding a core of fibrillar collagen. Moreover, increasing image resolution with Airyscan microscopy

Investigative Ophthalmology & Visual Science

revealed that glycoproteins in the vitreous fibrils are not distributed homogeneously along their length.

Our analysis of the geometric structure of vitreous fibrils in the mouse, based in 2D images did not provide much information on the matter, although it was clear that fibrils presented numerous branching points. Several questions remain open regarding collective geometric features of the mouse vitreous fibrils. On the one hand, it would be interesting to understand the spatial distribution of the fibrils within the vitreous. Questions worth addressing include the following. Do the fibrils form some sort of crystalline or symmetric pattern? Do they present special orientations with respect to the various eye structures or, rather, they appear isotropically distributed? How many fibrils per unit volume are there?

The presence of carbohydrates in the mouse vitreous has been documented in previous studies.[4,17,76] Rhodes (1982) investigated the existence of complex carbohydrates in the posterior vitreoretinal junction of the mouse eye.[28] Other researchers have identified hexosamines, such as N-acetyl glucosamine and N-acetyl galactosamine, as components of glycosaminoglycans present in the vitreous.[4,19,29,75] Our results provide the location of sugar residues in the mouse vitreous. We found that N-acetyl glucosamine or N-acetyl galactosamine are part of the vitreous fibrils, but, unlike findings in rabbits and humans,[56] no fucose residues were associated with retrolental or vitreoretinal vitreous fibrils in the mouse.

Hyaluronan is another carbohydrate extensively described in the eye.[60,70,77–82] In humans, HA is described as the predominant glycosaminoglycan in the vitreous.[17,34] In contrast, there is limited literature on its presence in the mouse vitreous. Hollyfield (1997) reported on the distribution of hyaluronate in mouse eye using bHABP[83] but did not clarify its presence or absence in the vitreous. HA polymers occur in various configurations and shapes, depending on factors such as size, salt concentration, pH, and associated cations.[84,85] In humans and other mammals, HA polymers infiltrate the vitreous fibrils. The combination of immobilized water and mutual electrostatic repulsion between HA polymers leads to the enlargement of the vitreous fibrillar scaffold, ultimately enhancing the viscosity of the vitreous.[61,86,87] Our study using lectins and b-HABP demonstrated that HA is a component of the vitreous fibrils, but it is not present in the interfibrillar space. This, along with the absence of proteins and carbohydrates in the interfibrillar space, may explain why the mouse vitreous is seemingly less viscous than human vitreous.

Despite the increasing use of intravitreal injections in ophthalmic treatments, studies evaluating their effects on ocular structures, such as the vitreous, remains limited. Previous reports have identified retinal detachment, cataract formation, and endophthalmitis as common complications.[88] The precise pathological processes triggered by intravitreal injections are still not fully understood, especially in the context of non-infectious situations. Our study suggests that even a mechanical injury produced by intravitreal injection induces an inflammatory response in the mouse vitreous, leading to increased fibril network density and macrophage/hyalocyte infiltration, as detected by Lamp1 immunostaining.

Despite that intravitreal injection injections are clinically safe in humans, our findings suggest that this mechanical injury can alter the vitreous balance, at least in mice, where the vitreous structure and composition differs from humans.

Previous research in mice has focused on intravitreal injection-associated complications in infectious models, such as the bacterial endophthalmitis model reported by Mursalin et al. (2022).[89] This model that mimics the human intravitreal injection documented significant IOP elevations following intravitreal injection. Furthermore, Meyer et al. (2023) reported that larger intravitreal injection volumes could significantly increase IOP, however, it is still uncertain whether vitreous composition plays a role in modulating these changes.[90]

The limitations of this study primarily arise from the use of 2D imaging techniques. Although these methods provide detailed insights into the fibrillar network; they may not fully capture the 3D complexity of vitreous architecture. Additionally, the intravitreal injections performed are not representative of those conducted in humans due to the excess volume injected in the small mouse vitreous. The technique used does not allow for precise quantification of the volume injected, introducing variability in the procedure. Furthermore, although a comprehensive range of histological and immunofluorescence techniques were used, the absence of in vivo imaging or functional assessments of the vitreous fibrils highlight an area for further exploration.

Acknowledgments

The authors thank Pablo Bueno Gómez for helpful discussions and assistance in this study.

Supported by the Ministerio de Ciencia e Innovación, Spain (grant number PID2021-122545OB-I00) and Fondo Europeo de Desarrollo Regional (FEDER).

Disclosure: **P. Jaramillo-Garcés**, None; **J. Pampalona**, None; **A. Carretero**, None; **E.J. Cunilleras**, None; **D. Ramos**, None; **J. Ruberte**, None

References

1. Brewton RG, Mayne R. Mammalian vitreous humor contains networks of hyaluronan molecules: electron microscopic analysis using the hyaluronan-binding region (G1) of aggrecan and link protein. *Exp Cell Res*. 1992;198(2):237–249.
2. Murthy KR, Goel R, Subbannayya Y, et al. Proteomic analysis of human vitreous humor. *Clin Proteomics*. 2014;11(1):29.
3. Ranchod TM, Goldenberg DT, Trese MT. The physiological consequences of vitreous composition. In: *Encyclopedia of the Eye*. New York, NY: Elsevier; 2010:439–443.
4. Le Goff MM, Bishop PN. Adult vitreous structure and postnatal changes. *Eye (Lond)*. 2008;22(10):1214–1222.
5. Sebag J, Balazs EA. Morphology and ultrastructure of human vitreous fibers. *Invest Ophthalmol Vis Sci*. 1989;30(8):1867–1871.
6. Bishop PN. Structural macromolecules and supramolecular organisation of the vitreous gel. *Prog Retin Eye Res*. 2000;19(3):323–344.
7. Fatt I. Hydraulic flow conductivity of the vitreous gel. *Invest Ophthalmol Vis Sci*. 1977;16(6):565–568.
8. Schulz A, Wahl S, Rickmann A, et al. Age-related loss of human vitreal viscoelasticity. *Transl Vis Sci Technol*. 2019;8(3):56.
9. Ito M, Nakashima M, Tsuchida N, Imaki J, Yoshioka M. Histogenesis of the intravitreal membrane and secondary vitreous in the mouse. *Invest Ophthalmol Vis Sci*. 2007;48(5):1923–1930.

10. Arciniegas A, Amaya LE. Bio-structural model of the human eye. *Ophthalmologica*. 1980;180(4):207–211.
11. Coulombre AJ, Coulombre JL. The role of intraocular pressure in the development of the chick eye: III. Ciliary body. *Am J Ophthalmol*. 1957;44(4 PART 2):85–93.
12. Cury CE, Jr, Rodrigues EB, Meyer CH, Farah ME. VEGF inhibitors and vitrectomy for diabetic vitreoretinopathy. *Dev Ophthalmol*. 2009;44:69–81.
13. Ihanamäki T, Pelliniemi LJ, Vuorio E. Collagens and collagen-related matrix components in the human and mouse eye. *Prog Retin Eye Res*. 2004;23(4):403–434.
14. Marshall GE, Konstas AG, Lee WR. Collagens in ocular tissues. *Br J Ophthalmol*. 1993;77(8):515–524. Erratum in: Br J Ophthalmol 1994 Jan;78(1):80.
15. Scott JE. The chemical morphology of the vitreous. *Eye (Lond)*. 1992;6(Pt 6):553–555.
16. Halfter W, Balasubramani M, Ring C, Schurer B. Cellular origin, formation and turnover of the vitreous. In: *Encyclopedia of the Eye*. New York, NY: Elsevier; 2010:233–237.
17. Bishop P. The biochemical structure of mammalian vitreous. *Eye* 1996;10:664–670.
18. Van Bockxmeer FM, Martin CE, Constable IJ. Iron-binding proteins in vitreous humour. *Biochim Biophys Acta*. 1983;758(1):17–23.
19. Breen M, Bizzell JW, Weinstein HG. A galactosamine containing proteoglycan in human vitreous. *Exp Eye Res*. 1977;24(4):409–412.
20. Wang Y, Yu G, Han Z, et al. Specificities of Ricinus communis agglutinin 120 interaction with sulfated galactose. *FEBS Lett*. 2011;585(24):3927–3934.
21. Reardon A, Heinegård D, Mcleod D, Sheehan JK, Bishop PN. The large chondroitin sulphate proteoglycan versican in mammalian vitreous. *Matrix Biology*. 1998;17(5):325–333.
22. Bishop PN, Takanosu M, Le Goff M, Mayne R. The role of the posterior ciliary body in the biosynthesis of vitreous humour. *Eye*. 2002;16(4):454–460.
23. Skeie JM, Roybal CN, Mahajan VB. Proteomic insight into the molecular function of the vitreous. *PLoS One*. 2015;10(5):e0127567.
24. Monteiro JP, Santos FM, Rocha AS, et al. Vitreous humor in the pathologic scope: insights from proteomic approaches. *Proteomics Clin Appl*. 2015;9(1–2):187–202.
25. Sebag J, Balazs EA. Human vitreous fibres and vitreoretinal disease. *Trans Ophthalmol Soc UK (1962)*. 1985;104(Pt 2):123–128.
26. Heffer A, Wang V, Sridhar J, et al. A mouse model of proliferative vitreoretinopathy induced by intravitreal injection of gas and RPE cells. *Transl Vis Sci Technol*. 2020;9(7):9.
27. Ihanamäki T, Salminen H, Säämänen AM, et al. Age-dependent changes in the expression of matrix components in the mouse eye. *Exp Eye Res*. 2001;72(4):423–431.
28. Rhodes RH. An ultrastructural study of the complex carbohydrates of the mouse posterior vitreoretinal juncture. *Invest Ophthalmol Vis Sci*. 1982;22(4):460–477.
29. Skeie JM, Mahajan VB. Proteomic interactions in the mouse vitreous-retina complex. *PLoS One*. 2013;8(11):e82140.
30. Skeie JM, Tsang SH, Mahajan VB. Evisceration of mouse vitreous and retina for proteomic analyses. *J Vis Exp*. 2011;50:2795.
31. Shi Y, Tu Y, De Maria A, Mecham RP, Bassnett S. Development, composition, and structural arrangements of the ciliary zonule of the mouse. *Invest Ophthalmol Vis Sci*. 2013;54(4):2504–2515.
32. Jones W, Rodriguez J, Bassnett S. Targeted deletion of fibrillin-1 in the mouse eye results in ectopia lentis and other ocular phenotypes associated with Marfan syndrome. *Dis Model Mech*. 2019;12(1):dmm037283.
33. Heffer A, Wang V, Sridhar J, et al. A mouse model of proliferative vitreoretinopathy induced by intravitreal injection of gas and RPE cells. *Transl Vis Sci Technol*. 2020;9(7):1–12.
34. Theocharis D, Skandalis S, Noulas A, Papageorgakopoulou N, Theocharis A, Karamanos N. Hyaluronan and chondroitin sulfate proteoglycans in the supramolecular organization of the mammalian vitreous body. *Connect Tissue Res*. 2008;49(3–4):124–128.
35. Grzybowski A, Told R, Sacu S, et al. 2018 Update on Intravitreal Injections: Euretina Expert Consensus Recommendations. *Ophthalmologica*. 2018;239(4):181–193.
36. Dossarps D, Bron AM, Koehrer P, et al. Endophthalmitis after intravitreal injections: Incidence, presentation, management, and visual outcome. *Am J Ophthalmol*. 2015;160(1):17–25.e1.
37. Anderson WJ, da Cruz NFS, Lima LH, Emerson GG, Rodrigues EB, Melo GB. Mechanisms of sterile inflammation after intravitreal injection of antiangiogenic drugs: a narrative review. *Int J Retina Vitreous*. 2021;7(1):37.
38. Greenberg JP, Belin P, Butler J, et al. Aflibercept-related sterile intraocular inflammation outcomes. *Ophthalmol Retina*. 2019;3(9):753–759.
39. Mitsuhashi J, Morikawa S, Shimizu K, Ezaki T, Yasuda Y, Hori S. Intravitreal injection of erythropoietin protects against retinal vascular regression at the early stage of diabetic retinopathy in streptozotocin-induced diabetic rats. *Exp Eye Res*. 2013;106:64–73.
40. Rittié L. Method for picrosirius red-polarization detection of collagen fibers in tissue sections. In: *Methods in Molecular Biology*. Vol. 1627. Totowa, NJ: Humana Press Inc.; 2017:395–407.
41. Schindelin J, Arganda-Carreras I, Frise E, et al. Fiji: An open-source platform for biological-image analysis. *Nat Methods*. 2012;9(7):676–682.
42. Bos KJ, Holmes DF, Meadows RS, Kadler KE, McLeod D, Bishop PN. Collagen fibril organisation in mammalian vitreous by freeze etch/rotary shadowing electron microscopy. *Micron*. 2001;32(3):301–306.
43. Keikhosravi A, Shribak M, Conklin MW, et al. Real-time polarization microscopy of fibrillar collagen in histopathology. *Sci Rep*. 2021;11(1):19063.
44. David AD, Parry JMS, eds. Subcellular Biochemistry. 1er. Ed. Vol. 82. *Fibrous Proteins: Structures and Mechanisms*. New York, NY: Springer; 2017: 458–483.
45. Bishop PN. Structural macromolecules and supramolecular organisation of the vitreous gel. *Prog Retin Eye Res*. 2000;19(3):323–344.
46. Ushiki T. Collagen fibers, reticular fibers and elastic fibers. a comprehensive understanding from a morphological viewpoint. *Arch Histol Cytol*. 2002;65(2):109–126.
47. Kaur J, Reinhardt DP. Extracellular matrix (ECM) molecules. In: *Stem Cell Biology and Tissue Engineering in Dental Sciences*. New York, NY: Elsevier Inc.; 2015:25–45.
48. George EL, Georges-Labouesse EN, Patel-King RS, Rayburn H, Hynes RO. Defects in mesoderm, neural tube and vascular development in mouse embryos lacking fibronectin. *Development*. 1993;119(4):1079–1091.
49. Singh P, Carraher C, Schwarzbauer JE. Assembly of fibronectin extracellular matrix. *Annu Rev Cell Dev Biol*. 2010;26:397–419.
50. Libby RT, Champliaud MF, Claudepierre T, et al. Laminin expression in adult and developing retinae: evidence of two novel CNS laminins. *J Neurosci*. 2000;20(17):6517–6528.
51. Hirrlinger PG, Pannicke T, Winkler U, et al. Genetic deletion of laminin isoforms $\beta 2$ and $\gamma 3$ Induces a reduction in Kir4.1 and aquaporin-4 expression and function in the retina. *PLoS One*. 2011;6(1):e16106.

Investigative Ophthalmology & Visual Science

52. Timpl R, Wiedemann H, van Delden V, Furthmayr H, Kühn K. *A network model for the organization of type IV collagen molecules in basement membranes*. *Eur J Biochem*. 1981;120(2):203–211.
53. Harold Davenport. 2015.*Histological-And-Histochemical-Technics*. 1er Ed. Philadelphia, PA: Saunders, 1960. 321–326.
54. Piller V, Piller F, Cartron J-P. Comparison of the carbohydrate-binding specificities of seven N-acetyl-D-galactosamine-recognizing lectins. *Eur J Biochem*. 1990;191(2):461–466.
55. Adibekian A, Von der Lieth CW, Seeberger PH. Exploring the structural diversity of mammalian carbohydrates ("glycospace") by statistical databank analysis. *ACS Chem Biol*. 2007;2(10):685–691.
56. Rhodes RH. A comparative study of vitreous-body and zonular glycoconjugates that bind to the lectin from Ulex europaeus. *Histochemistry*. 1983;78(3):349–360.
57. Bojar D, Meche L, Meng G, et al. A useful guide to lectin binding: machine-learning directed annotation of 57 unique lectin specificities. *ACS Chem Biol*. 2022;17(11):2993–3012.
58. Rodrigues ML, Alvarez M, Fonseca FL, Casadevall A. Binding of the wheat germ lectin to Cryptococcus neoformans suggests an association of chitinlike structures with yeast budding and capsular glucuronoxylomannan. *Eukaryot Cell*. 2008;7(4):602–609.
59. Toole BP. Hyaluronan and its binding proteins, the hyaladherins. *Curr Opin Cell Biol*. 1990;2(5):839–844.
60. Osterlin SE, Jacobson B. The synthesis of hyaluronic acid in vitreous. I. Soluble and particulate transferases in hyalocytes. *Exp Eye Res*. 1968;7(4):497–510.
61. Selyanin MA, Boykov PY, Khabarov VN. Molecular and Supramolecular Structure of Hyaluronic Acid. In: *Hyaluronic Acid*. Hoboken, NJ: Wiley; 2015:97–119.
62. Cowman MK, Matsuoka S. The intrinsic viscosity of hyaluronan. In: *Hyaluronan*. New York, NY: Elsevier; 2002:75–78.
63. Sodhi H, Panitch A. Glycosaminoglycans in tissue engineering: a review. *Biomolecules*. 2021;11(1):1–22.
64. Cowman MK, Lee HG, Schwertfeger KL, McCarthy JB, Turley EA. The content and size of hyaluronan in biological fluids and tissues. *Front Immunol*. 2015;6:261.
65. Wei Q, Zhang T, Jiang R, et al. Vitreous fibronectin and fibrinogen expression increased in eyes with proliferative diabetic retinopathy after intravitreal anti-VEGF therapy. *Invest Ophthalmol Vis Sci*. 2017;58(13):5783–5791.
66. Dong S, Hughes RC. Macrophage surface glycoproteins binding to galectin-3 (Mac-2-antigen). *Glycoconj J*. 1997;14(2):267–74.
67. Boneva SK, Wolf J, Rosmus DD, et al. Transcriptional profiling uncovers human hyalocytes as a unique innate immune cell population. *Front Immunol*. 2020;11:567274.
68. Schwake M, Schröder B, Saftig P. Lysosomal membrane proteins and their central role in physiology. *Traffic*. 2013;14(7):739–748.
69. Saftig P, Klumperman J. Lysosome biogenesis and lysosomal membrane proteins: trafficking meets function. *Nat Rev Mol Cell Biol*. 2009;10(9):623–635.
70. Bremer FM, Rasquin F. Histochemical localization of hyaluronic acid in vitreous during embryonic development. *Invest Ophthalmol Vis Sci*. 1998;39(12):2466–2469.
71. Bos KJ, Holmes DF, Kadler KE, McLeod D, Morris NP, Bishop PN. Axial structure of the heterotypic collagen fibrils of vitreous humour and cartilage. *J Mol Biol*. 2001;306(5):1011–1022.
72. Bishop PN, Crossman MV, McLeod D, Ayad S. Extraction and characterization of the tissue forms of collagen types II and IX from bovine vitreous. *Biochem J*. 1994;299(Pt 2):497–505.
73. Shi Y, Tu Y, De Maria A, Mecham RP, Bassnett S. Development, composition, and structural arrangements of the ciliary zonule of the mouse. *Invest Ophthalmol Vis Sci*. 2013;54(4):2504–2515.
74. Bishop PN, McLeod D, Reardon A. Effects of hyaluronan lyase, hyaluronidase, and chondroitin ABC lyase on mammalian vitreous gel. *Invest Ophthalmol Vis Sci*. 1999;40(10):2173–2178.
75. Kinsey R, Williamson MR, Chaudhry S, et al. Fibrillin-1 microfibril deposition is dependent on fibronectin assembly. *J Cell Sci*. 2008;121(16):2696–2704.
76. Brewton RG, Mayne R. Mammalian vitreous humor contains networks of hyaluronan molecules: Electron microscopic analysis using the hyaluronan-binding region (G1) of aggrecan and link protein. *Exp Cell Res*. 1992;198(2):237–249.
77. Mishra D, Gade S, Glover K, Sheshala R, Singh TRR. Vitreous humor: composition, characteristics and implication on intravitreal drug delivery. *Curr Eye Res*. 2023;48(2):208–218.
78. Sebag J, Yee KMP. Chapter 16 Vitreous: From Biochemistry to Clinical Relevance. Available at: https://api.semanticscholar.org/CorpusID:2736032
79. Noulas AV, Theocharis AD, Feretis E, Papageorgakopoulou N, Karamanos NK, Theocharis DA. Pig vitreous gel: macromolecular composition with particular reference to hyaluronan-binding proteoglycans. *Biochimie*. 2002;84(4):295–302.
80. Schwartz DM, Shuster S, Jumper MD, Chang A, Stern R. Human vitreous hyaluronidase: isolation and characterization. *Curr Eye Res*. 1996;15(12):1156–1162.
81. Itakura H, Kishi S, Kotajima N, Murakami M. Decreased vitreal hyaluronan levels with aging. *Ophthalmologica*. 2009;223(1):32–35.
82. Grimshaw J, Kane Á, Trocha-Grimshaw J, Douglas A, Chakravarthy U, Archer D. Quantitative analysis of hyaluronan in vitreous humor using capillary electrophoresis. *Electrophoresis*. 1994;15(1):936–940.
83. Hollyfield JG, Rayborn ME, Tammi R. Hyaluronan localization in tissues of the mouse posterior eye wall: absence in the interphotoreceptor matrix. *Exp Eye Res*. 1997;65(5):603–608.
84. Laurent TC, Fraser JR. Hyaluronan. *FASEB J*. 1992;6(7):2397–2404.
85. Evered D, Whelan J, eds. The biology of hyaluronan. *Ciba Found Symp*. 1989;143:1–298. Available at: https://download.e-bookshelf.de/download/0000/5742/10/L-G-0000574210-0002288091.pdf.
86. Casey-Power S, Ryan R, Behl G, McLoughlin P, Byrne ME, Fitzhenry L. Hyaluronic acid: its versatile use in ocular drug delivery with a specific focus on hyaluronic acid-based polyelectrolyte complexes. *Pharmaceutics*. 2022;14(7):1479.
87. de la Motte CA, Drazba JA. Viewing hyaluronan: Imaging contributes to imagining new roles for this amazing matrix polymer. *J Histochem Cytochem*. 2011;59(3):252–257.
88. van der Reis MI, La Heij EC, De Jong-Hesse Y, Ringens PJ, Hendrikse F, Schouten JS. A systematic review of the adverse events of intravitreal anti-vascular endothelial growth factor injections. *Retina*. 2011;31(8):1449–1469.
89. Mursalin MH, Livingston E, Coburn PS, Miller FC, Astley R, Callegan MC. Intravitreal injection and quantitation of infection parameters in a mouse model of bacterial endophthalmitis. *Vis Exp*. 2021;168, https://doi.org/10.3791/61749.
90. Meyer CH, Melo GB, Khanani AM. Can intravitreal injections with higher volume cause higher intraocular eye pressure? Considerations for anti-complement injections in normal and glaucomatous eyes. *Int J Retina Vitreous*. 2023;9(1):80.

Investigative Ophthalmology & Visual Science